Tryptophan-mediated charge-resonance stabilization in the *bis*-Fe(IV) redox state of MauG

Jiafeng Geng[a], Kednerlin Dornevil[a], Victor L. Davidson[b], and Aimin Liu[a,1]

[a]Department of Chemistry, Center for Diagnostics and Therapeutics, and Molecular Basis of Disease Program, Georgia State University, Atlanta, GA 30303; and [b]Burnett School of Biomedical Sciences, College of Medicine, University of Central Florida, Orlando, FL 32827

Edited by Harry B. Gray, California Institute of Technology, Pasadena, CA, and approved May 8, 2013 (received for review January 24, 2013)

The diheme enzyme MauG catalyzes posttranslational modifications of a methylamine dehydrogenase precursor protein to generate a tryptophan tryptophylquinone cofactor. The MauG-catalyzed reaction proceeds via a *bis*-Fe(IV) intermediate in which one heme is present as Fe(IV)=O and the other as Fe(IV) with axial histidine and tyrosine ligation. Herein, a unique near-infrared absorption feature exhibited specifically in *bis*-Fe(IV) MauG is described, and evidence is presented that it results from a charge-resonance-transition phenomenon. As the two hemes are physically separated by 14.5 Å, a hole-hopping mechanism is proposed in which a tryptophan residue located between the hemes is reversibly oxidized and reduced to increase the effective electronic coupling element and enhance the rate of reversible electron transfer between the hemes in *bis*-Fe(IV) MauG. Analysis of the MauG structure reveals that electron transfer via this mechanism is rapid enough to enable a charge-resonance stabilization of the *bis*-Fe(IV) state without direct contact between the hemes. The finding of the charge-resonance-transition phenomenon explains why the *bis*-Fe(IV) intermediate is stabilized in MauG and does not permanently oxidize its own aromatic residues.

charge transfer | electron hopping | high-valent iron | metalloprotein | tryptophan radical

It has long been known that under certain conditions, aromatic hydrocarbon cation radicals may interact with their parent neutral molecules in a face-to-face manner to generate noncovalent cation radical dimers, which present a unique electronic absorption band in the near-infrared (NIR) region (1). The NIR spectral feature is a characteristic property of resonance stabilization of the spin and charge within the dimeric complexes and therefore is termed a charge-resonance (CR) band. The CR-transition phenomenon has been studied in various organic model systems with conjugated structures (2–6); however, it is observed rarely in biological systems. A literature review revealed only one example, i.e., the radical cation of the primary electron donor P (known as the "special pair") in bacterial photosynthetic reaction centers (7, 8). Here, we present evidence for a CR-transition phenomenon arising from a system consisting of two protein-bound hemes and a tryptophan residue in a diheme enzyme, MauG, encoded by the *mauG* gene (9).

MauG catalyzes the final steps in the biosynthesis of the catalytic tryptophan tryptophylquinone (TTQ) cofactor of methylamine dehydrogenase (MADH). MauG uses two *c*-type hemes for oxidative posttranslational modifications of a precursor protein, preMADH, to generate TTQ (10). Spectroscopic and structural studies of MauG revealed the presence of a five-coordinate, high-spin heme with an axial histidine coordination (denoted as $Heme_{5C}$) and a six-coordinate, low-spin heme with an unusual axial histidine–tyrosine coordination (denoted as $Heme_{6C}$) in the resting diferric state (Fig. 1*A*) (10, 11). The two Fe ions in MauG are separated by 21.1 Å, with the closest distance between the porphyrin rings being 14.5 Å (10). Importantly, only $Heme_{5C}$ is reactive toward exogenous small molecules because of its coordination vacancy (11). MauG-catalyzed TTQ biosynthesis is accomplished through radical chemistry via a three-step, six-electron oxidation process; each step can be initiated using 1 eq of H_2O_2 as the oxidant (Fig. 1*B*) (12). Our recent work has shown that each two-electron oxidation reaction proceeds via a high-valence *bis*-Fe(IV) intermediate, in which $Heme_{5C}$ is present as Fe(IV)=O, and $Heme_{6C}$ as Fe(IV) with the axial histidine–tyrosine ligand set retained (Fig. 1*C*) (13).

Although the two hemes in MauG are physically separated, they share electrons efficiently (11). Redox titrations revealed that the diheme system exhibits redox cooperativity, with the two hemes behaving as a single diheme unit rather than as independent hemes (14). A tryptophan residue, Trp93, is positioned midway between the hemes without direct covalent or hydrogen-bonding interactions with either heme (Fig. 1*A*). Previously, we reported the presence of a radical species detectable by EPR spectroscopy within the same time window as the one in which the *bis*-Fe(IV) species was observed (13). This radical species, representing only a few percent of the oxidized protein, was proposed to be located on Trp93 (13).

Despite being a highly potent oxidant, the *bis*-Fe(IV) species displays extraordinary stability in the absence of preMADH, with a half-life of several minutes (13, 15), rather than permanently oxidizing its own aromatic residues, such as Trp93, Trp199, and the heme ligand Tyr294. In this study, an NIR electronic absorption feature was observed in *bis*-Fe(IV) MauG. This spectral feature is characteristic of a CR-transition phenomenon. Evidence is presented that the transition process occurs in the absence of direct heme–heme contact by ultrafast and reversible electron transfer (ET) between the two high-valent hemes, via hole hopping through the intervening Trp93 residue. This finding reveals the chemical basis for the stability of the *bis*-Fe(IV) species.

Results and Discussion

Spectroscopic Signature of *bis*-Fe(IV) MauG in the NIR Region. The NIR region of the electronic absorption spectrum of the *bis*-Fe(IV) species was not explored in previous studies (13, 15, 16). Inspection of this region revealed that a broad band centered at 950 nm developed upon addition of H_2O_2 to diferric MauG concomitant with the previously observed changes in the visible region of the spectrum (Fig. 2*A*). No such absorption feature in the NIR region was observed in the spectra of either diferric or diferrous MauG. Parallel experiments were performed in a D_2O-based buffer to avoid interference from H_2O, which has intense NIR absorption over 1,300 nm. The peak at 950 nm was unchanged in the D_2O buffer, and no additional features were observed at longer wavelengths (Fig. 2*B*). The intensity of the NIR band was maximized by adding 10 eq of H_2O_2 to MauG. This ratio is consistent with the result of a recent X-ray absorption study, which reported a near-complete conversion from diferric to *bis*-Fe(IV) MauG after addition of 10 eq of H_2O_2 (17). At the 10:1 ratio of $[H_2O_2]$ to [MauG], a plot of the intensity of the NIR band against [MauG] was linear, with a slope of $7.0 \pm 0.1 \times 10^3\ M^{-1}\cdot cm^{-1}$ (Fig. 2*B*), equal to the molar absorptivity of the *bis*-Fe(IV) species at 950 nm, assuming complete conversion from the diferric state. Notably, in

Author contributions: J.G. and A.L. designed research; J.G., K.D., and A.L. performed research; V.L.D. contributed new reagents/analytic tools; J.G., K.D., and A.L. analyzed data; and J.G., V.L.D., and A.L. wrote the paper.

The authors declare no conflict of interest.

This article is a PNAS Direct Submission.

[1]To whom correspondence should be addressed. E-mail: feradical@gsu.edu.

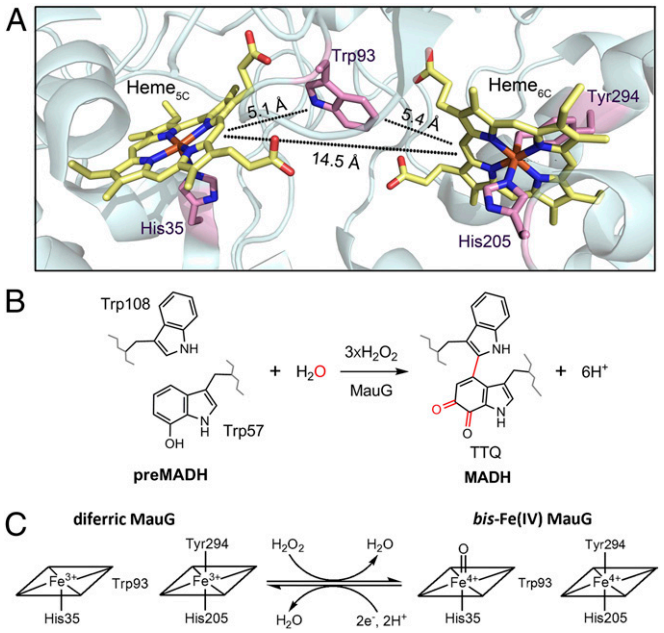

Fig. 1. Diheme center of MauG and its *bis*-Fe(IV) intermediate. (*A*) Relative orientation of hemes and the intervening tryptophan residue [Protein Data Bank (PDB) ID code 3L4M]. The edge-to-edge distances between the indole side chain of Trp93 and each heme porphyrin ring, and between the two heme porphyrin rings, are indicated. (*B*) MauG-dependent TTQ biosynthesis. Posttranslational modifications of preMADH are shown in red. (*C*) Chemical conversion between diferric and *bis*-Fe(IV) MauG.

some synthetic Fe(IV)=O complexes, broad NIR electronic absorption bands in the range of 700–1,000 nm have been observed (18). A subsequent study revealed that these bands originate from *d-d* transitions of the high-valence Fe ions (19). Such spectral features rarely are reported in biological ferryl systems because the molar absorptivities of absorption bands caused by *d-d* transitions are very low (5–500 $M^{-1}{\cdot}cm^{-1}$) (20). As the molar absorptivity of the NIR band observed in *bis*-Fe(IV) MauG is much larger, it must have a different molecular origin.

In the visible region of the spectrum, formation of *bis*-Fe(IV) MauG altered both the Soret peak and the Q-bands. The Soret peak exhibited a 4-nm red-shift and decreased intensity, whereas the Q-bands presented two new peaks at 526 and 559 nm (Fig. 2*A*). These spectral changes were more pronounced with the optimized 10:1 ratio of H_2O_2 than with the stoichiometric ratio used in prior studies (15, 16), consistent with a more complete formation of the *bis*-Fe(IV) species. The absorption maxima for the newly developed Q-bands are similar to those observed in ferryl species from nonglobin peroxidases, such as cytochrome *c* peroxidase (21) and horseradish peroxidase (22), but are different from those reported for ferryl species from globins (540–545 and 580–590 nm) (23). Addition of H_2O_2 also resulted in the emergence of a very minor spectral feature in the 600–700-nm region, with the absorption maximum at 664 nm (Fig. 2*B*). An absorption peak in this region is characteristic of a compound I species (24), defined as Fe(IV) heme coupled to a porphyrin cation radical, suggesting that a small portion of the high-valent MauG is in a compound I-like state.

It was shown previously that although *bis*-Fe(IV) MauG is relatively stable, it may be converted rapidly to diferric MauG by addition of the substrate protein, preMADH (13). In Fig. 3*A*, the *bis*-Fe(IV) species was first generated by mixing diferric MauG with 1 eq of H_2O_2, followed by mixing with 1 eq of preMADH. After the second mix, the *bis*-Fe(IV) species immediately decayed to the diferric state, as evidenced by the return of the heme Soret and Q-bands to the initial resting state. The simultaneous disappearance of the NIR band confirms that this signal is a spectral feature of *bis*-Fe(IV) MauG (Fig. 3*A*). Furthermore, in the absence of preMADH, the rate of decay of the NIR band is very similar to the rate of change in the Soret peak that correlates with the decay of the *bis*-Fe(IV) species (Fig. 3 *B* and *C*).

Three previously structurally characterized MauG variants also were tested in this study. Upon reaction with H_2O_2, the same NIR band was observed in W199F (Fig. 3*D*) and P107V MauG (Fig. 3*E*). Both variants were shown to be capable of stabilizing the *bis*-Fe(IV) species (25, 26). In contrast, the NIR spectral feature was not observed in Y294H MauG upon addition of H_2O_2 (Fig. 3*F*). Tyr294 is one of the axial ligands of $Heme_{6C}$ (10). In Y294H MauG, $Heme_{6C}$ has an axial *bis*-histidine coordination, and the *bis*-Fe(IV) intermediate is not generated (16). Instead, this mutant stabilizes a compound I-like species with a characteristic absorption band at 655 nm after H_2O_2 treatment (16). These results validate the association of the NIR spectral feature with the *bis*-Fe(IV) state rather than just any ferryl species.

Origin of the NIR Spectral Feature: Model for CR Stabilization of *bis*-Fe(IV) MauG. A molecular orbital (MO) diagram for the CR complex of a mixed-valence cation radical $(\Pi)_2^{+\bullet}$ is shown in Fig. 4*A*. The CR stabilization energy (ΔE_{CR}) originates from exchange interactions between the molecular orbitals of each monomer and subsequent delocalization of the spin and charge over a greater number of atoms. The CR band ($h\upsilon_{CR}$) typically is observed in the NIR region, and it is a characteristic signature of resonance stabilization of spin and charge within the CR complex. Kochi and coworkers (3–5) investigated the ET process between the two monomer units in the CR systems and demonstrated that a CR transition can proceed via through-space or through-bond ET. The former requires parallel alignment and close proximity of the monomers to allow direct interaction between their π-orbitals; the latter requires covalent linkage of the monomers by suitable bridging structures serving as an "electric wire" to efficiently shuttle the spin and charge between them. In both cases, ultrafast and reversible ET with rate constants in the range of

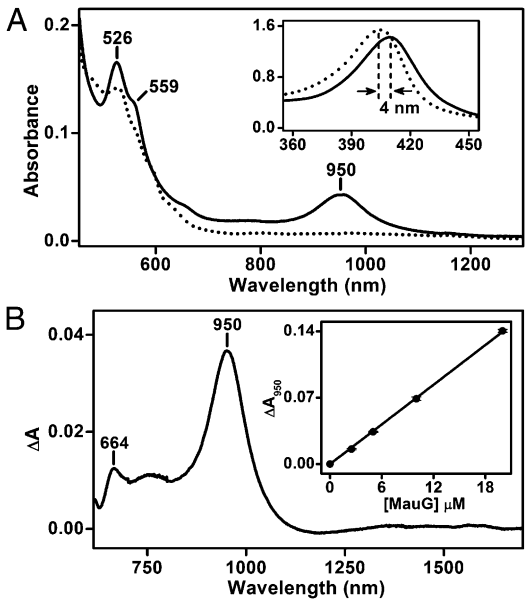

Fig. 2. The *bis*-Fe(IV) state of MauG exhibits a spectral feature in the NIR region. (*A*) Vis-NIR spectra of MauG (5 μM) before (dotted trace) and after (solid trace) addition of 10 eq of H_2O_2. (*Inset*) Expanded view of the Soret region. (*B*) Vis-NIR difference spectrum of MauG (5 μM) obtained in D_2O-based buffer by subtracting the initial spectrum of diferric MauG from the one after addition of 10 eq of H_2O_2. (*Inset*) Absorption change at 950 nm (ΔA_{950}) as a function of [MauG], with the ratio of [H_2O_2] to [MauG] kept at 10:1. The solid line is the linear fit of the experimental data.

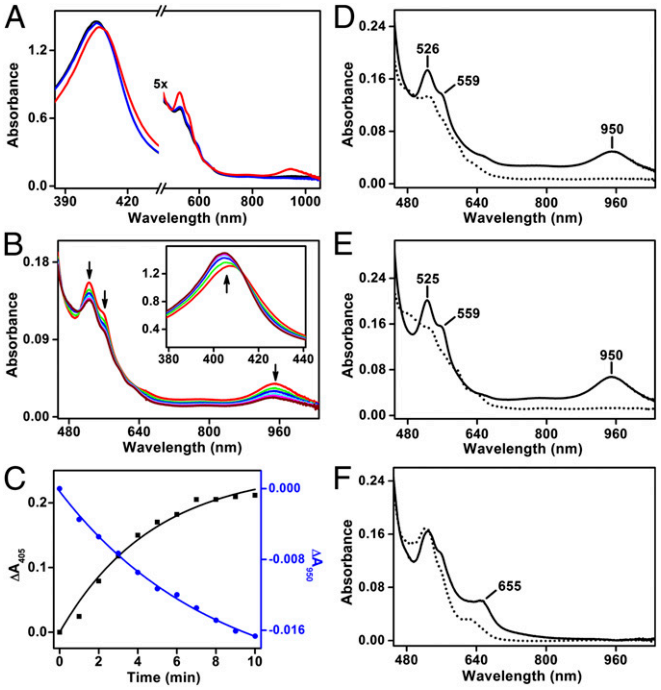

Fig. 3. The NIR spectral feature is specific for the *bis*-Fe(IV) state of MauG. (*A*) Absorption spectra of diferric MauG (5 μM, black trace) after sequential mixing with 1 eq of H_2O_2 (red trace) and 1 eq of preMADH (blue trace). The black and blue traces are nearly identical. (*B*) Time-resolved spectra for the spontaneous decay of *bis*-Fe(IV) MauG in the absence of preMADH. The spectra were recorded every 2 min for 10 min after addition of 10 eq of H_2O_2 to diferric MauG (5 μM). (*Inset*) Expanded view of the Soret region. ↑ and ↓, trends of changes in the spectra. (*C*) Time courses for the changes in absorbance at 405 nm (■) and 950 nm (blue ●) within the same time window as in *B*. The solid lines represent fits of the experimental data to a single exponential rise/decay. (*D*) Absorption spectra of W199F before (dotted trace) and after (solid trace) addition of 10 eq of H_2O_2. (*E*) Absorption spectra of P107V before (dotted trace) and after (solid trace) addition of 10 eq of H_2O_2. (*F*) Absorption spectra of Y294H before (dotted trace) and after (solid trace) addition of 10 eq of H_2O_2.

10^7–10^{11} s^{-1} frequently is observed and suggested to be essential for delocalization of the spin and charge within the CR complexes (3–5, 27).

Resonance stabilization of the spins and charges also has been observed in the binuclear dication diradical complex of $(\Pi^{+\bullet})_2$ (Fig. 4*B*) (4, 28–33). We term the former case with an odd number of spin/charge as type I CR and the latter case with an even number as type II CR. Notably, both types of CR-transition phenomena may be observed from the same system and further distinguished by the relative positions of their CR bands (4, 31–33). Despite the inherent energy penalty caused by electrostatic repulsion in the doubly charged complex, the ΔE_{CR} value of type II CR usually is larger than that of type I CR from the same system, which causes a blue-shift of the CR band of the $(\Pi^{+\bullet})_2$ complex compared with the $(\Pi)_2{}^{+\bullet}$ complex (4, 31–33). In principle, both types of CR complexes bear a close relationship to the conventional charge-transfer complexes derived from closed-shell diamagnetic precursors consisting of electron-rich donors and electron-poor acceptors. The assembly of type II CR complexes may be considered from an alternative perspective that starts from a pair of closed-shell species such as a dication and its parent neutral molecule (32, 34).

Through one electron oxidation of zinc octaethylporphyrin, Fuhrhop et al. generated cation porphyrin radical derivatives that self-assembled to produce dimeric complexes displaying a broad NIR absorption band centered around 950 nm (30). Similar phenomena were reported for the radical derivatives of some other metalloporphyrins (29, 31). Subsequent crystallization studies demonstrated that the cation porphyrin radicals formed tight dimeric complexes in a face-to-face manner with an interplanar separation distance smaller than 3.5 Å (35). The spectral characteristics and molar absorptivity of the NIR band observed in *bis*-Fe(IV) MauG are highly reminiscent of the CR bands from these metalloporphyrin complexes. In MauG, the two oxidizing equivalents derived from H_2O_2 are distributed within the diheme system as two positive charges, giving rise to the *bis*-Fe(IV) redox state. This is electronically equivalent to two ferric hemes, each coupled with a porphyrin cation radical, a scenario resembling the binuclear dication diradical complex of $(\Pi^{+\bullet})_2$ in type II CR. The observed NIR spectral feature in MauG likely is not the result of type I-like CR in a one-electron reduced system of *bis*-Fe(IV), i.e., [Fe(IV)•••Fe(III)] ↔ [Fe(III)•••Fe(IV)], in which case one would expect the CR band to be located at a wavelength much longer than 950 nm (8, 9, 32, 33, 36). For the diheme system of MauG, the critical question is how the CR-transition phenomenon originates when the two hemes are physically separated by 14.5 Å and have no covalent bridging structures between them.

Trp93, which resides midway between the hemes (Fig. 1*A*), is proposed to be critical for the occurrence of this seemingly inexplicable CR-transition phenomenon in *bis*-Fe(IV) MauG. Each Fe(IV) heme is a sufficiently strong oxidant to oxidize Trp93, as evidenced by the observation that a minor radical species is always observed along with *bis*-Fe(IV) MauG (13). Although Trp93 can donate an electron to either of them, it cannot fill two holes simultaneously. Thus, it is proposed that hole hopping via Trp93 is involved in the reversible ET process between the hemes to enable CR stabilization of *bis*-Fe(IV) MauG. This residue would need to be reversibly oxidized and reduced, at a sufficiently fast speed to facilitate CR transition by increasing the effective electron coupling element while decreasing the effective ET distance.

Because neither of the previously discussed CR mechanisms (type I or II) satisfactorily applies to the phenomenon in MauG, we propose a type III class whereby ET between the two interacting moieties in the CR complex is facilitated by electron/hole hopping through a third π system (i.e., Trp93 in this biological case). The proposed resonance structures that give rise to the CR stabilization of *bis*-Fe(IV) MauG are shown in Fig. 4*C* and represent the first type III CR model. Among the resonance structures of two-electron oxidized MauG, the *bis*-Fe(IV) resonance structure is most stable and was confirmed as the dominant species by our previous spectroscopic studies (13). The type III CR model is consistent with the observation that a minor radical species was detected by EPR spectroscopy concomitant with the observation of the *bis*-Fe(IV) species (13). This radical species now is attributed to the existence of the compound (Cpd) ES, defined as Fe(IV) heme coupled to an amino acid based radical, and Cpd ES′ resonance structures in the CR system with the radical located at Trp93. Moreover, the appearance of the additional minor absorption peak at 664 nm upon addition of H_2O_2 to diferric MauG (Fig. 2*B*) suggests that a small amount of compound I-like species exists in the CR system. Our previous Mössbauer characterization of the reaction mixture of MauG and H_2O_2 revealed that other than the *bis*-Fe(IV) and Fe(III) species, a minor portion of other heme species was present (13). The spin-coupled compound I-like species, such as Cpd I and Cpd I′ in the CR model, are reasonable candidates.

In the proposed type III CR model, the spins and charges are delocalized within a ternary system composed of two hemes and one tryptophan residue spanning over 20 Å. Notably, both Cpd ES and Cpd ES′ in the model contain a cation radical form of Trp93, the residue proposed to be the hopping site. Such radical intermediates in a hopping mechanism are expected to be transient and rarely have been detected. One example is the observation of a $Trp^{\bullet+}$ hopping intermediate formed during activation of the R2 subunit of *Escherichia coli* class I ribonucleotide reductase (37) and another in a mutant protein of DNA photolyase (38). In the type III CR system of *bis*-Fe(IV) MauG, the hopping

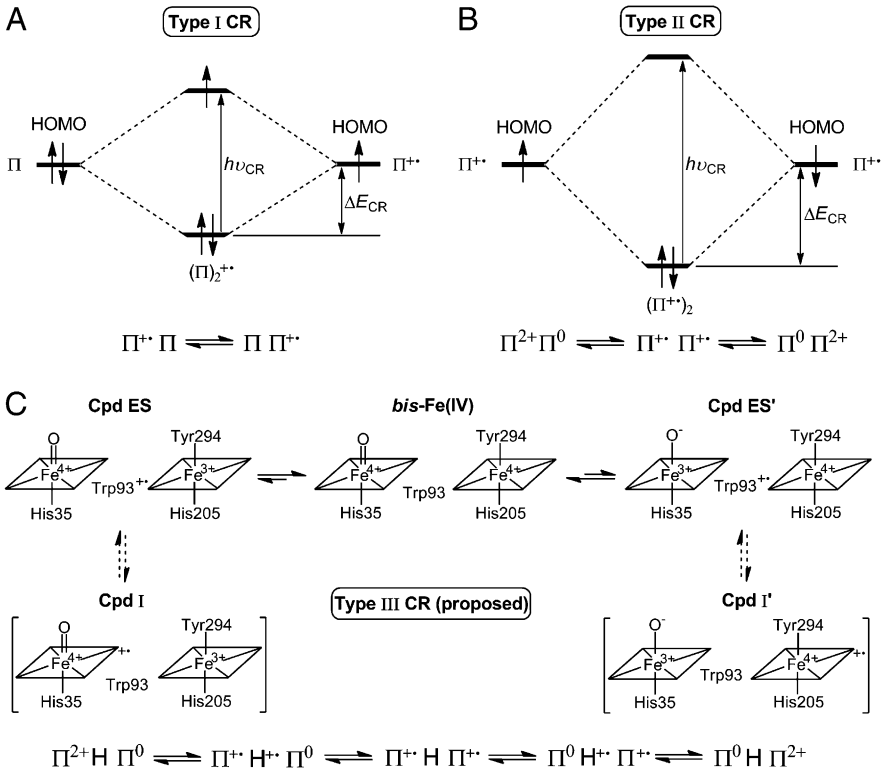

Fig. 4. CR stabilization of *bis*-Fe(IV) MauG. Qualitative MO diagrams and resonance structures are described for noncovalent dimeric complexes of (*A*) type I CR in the mixed-valence cation radical $(\Pi)_2^{+\bullet}$ and (*B*) type II CR in the dication diradical $(\Pi^{+\bullet})_2$. The origins of the CR stabilization energy (ΔE_{CR}) and CR bands ($h\upsilon_{CR}$) are illustrated. (*C*) Proposed resonance structures for type III CR in the *bis*-Fe(IV) redox state of MauG. The spins and charges are delocalized throughout the diheme system and stabilized via a series of CR structures with "*bis*-Fe(IV)" as the dominant one. H, hopping site.

intermediates are long-lived because of the reversibility of ET that allows resonance stabilization of the spins and charges.

Mechanism of ET Between the Hemes in *bis*-Fe(IV) MauG. Ultrafast and reversible ET between the two interacting moieties is essential for a CR-transition phenomenon. Unfortunately, it is not possible to directly monitor the ET rate between the hemes in *bis*-Fe(IV) MauG. The formation of the *bis*-Fe(IV) species upon addition of H_2O_2 is complete within the dead-time of stopped-flow mixing (~2–3 ms) (15). Furthermore, the spectral changes in the two hemes are complementary and there is no net change in the absorbance spectrum that can be monitored. It is possible, however, to estimate the ET rate and determine the likely ET mechanism from analysis of the MauG structure in the context of ET theory (39).

ET between redox centers can proceed via two different mechanisms, single-step electron tunneling or multistep hopping (39, 40). In the former case, there is no change in the redox state of the conductive medium. In contrast, if hopping is involved in ET, certain elements of the medium will be reversibly oxidized and reduced. In a hopping mechanism, the electron that leaves the electron donor is not the same as the one that enters the electron acceptor. Rather, it is an electron displaced from the hopping site. The observed ET rate is determined by the rate of the slowest "hop," which typically is much faster than that of the corresponding direct single-step tunneling reaction. For a single-step tunneling pathway or an individual segment of a multistep hopping pathway, the ET rate (k_{ET}) is described by Eq. **1** (39). At a given temperature, k_{ET} varies predictably with the driving force ($\Delta G°$), determined from ΔE_m of the ET reaction, the reorganization energy (λ) comprising the inner-sphere and outer-sphere nuclear rearrangement, and the electronic coupling element (H_{AB}). H_{AB} depends on the ET distance and the nature of the intervening medium between the donor and acceptor, as shown in Eq. **2** (40), in which β is the decay constant, a parameter that quantifies the efficiency of the medium in mediating ET, r is the distance between the donor and acceptor, r_0 is the close contact distance (the sum of van der Waals radii), and $H_{AB}(r_0)$ is the electronic coupling element at $r = r_0$.

$$k_{ET} = \left[4\pi^2 H_{AB}^2 \Big/ h(4\pi\lambda RT)^{0.5}\right] \exp\left[-(\Delta G^0 + \lambda)^2 \Big/ 4\lambda RT\right] \quad [1]$$

$$H_{AB} = H_{AB}(r_0)\exp[-0.5\beta(r - r_0)] \quad [2]$$

The HARLEM program (see *Methods*) was used to calculate H_{AB} and β values for ET reactions in MauG using its crystal structure (10). These values were calculated for the single-step electron tunneling pathway between the hemes and the electron tunneling segments between Trp93 and each heme, the latter of which are parts of the proposed hopping mechanism for CR stabilization of *bis*-Fe(IV) MauG. Table 1 shows that each of the two hopping segments exhibits an H_{AB} value that is 10^3-fold greater than that of the single-step tunneling reaction. As $k_{ET} \propto H_{AB}^2$, in the absence of other changes k_{ET} of the hopping-mediated ET is expected to be six orders of magnitude larger than that of the single-step direct tunneling mechanism.

The HARLEM analysis did not take into account the effects of $\Delta G°$ and λ on the rate of ET. Using the method developed by Gray and coworkers (40), hopping maps were constructed for the

Table 1. HARLEM analysis of ET reactions in MauG

ET route	*r*, Å*	β, Å^{-1}	H_{AB}†
Single-step tunneling, between $Heme_{6C}$ and $Heme_{5C}$	14.5	1.40	3.8×10^{-5}
Segments of Trp93-mediated hopping			
Between $Heme_{6C}$ and Trp93	5.4	1.24	3.7×10^{-2}
Between Trp93 and $Heme_{5C}$	5.1	1.29	3.8×10^{-2}

The calculation was performed using the crystal structure of MauG (PDB ID code 3L4M).
*r is the direct (edge-to-edge) distance between redox centers.
†H_{AB} is in dimensionless units for relative comparison.

Table 2. Predicted ET rates from the hopping maps

Electron donor	λ, eV	$k_{hopping}$, s^{-1}*	$k_{tunneling}$, s^{-1}*,†
$Heme_{6C}$	0.6	5.2×10^7 to 4.0×10^9	7.3×10^3 to 4.9×10^4
$Heme_{6C}$	0.8	7.2×10^6 to 5.0×10^8	8.5×10^2 to 6.5×10^3
$Heme_{6C}$	1.0	1.0×10^6 to 6.1×10^7	1.1×10^2 to 9.0×10^2
$Heme_{5C}$	0.6	5.7×10^7 to 3.9×10^9	7.3×10^3 to 4.9×10^4
$Heme_{5C}$	0.8	8.0×10^6 to 4.9×10^8	8.5×10^2 to 6.5×10^3
$Heme_{5C}$	1.0	1.0×10^6 to 6.3×10^7	1.1×10^2 to 9.0×10^2

Ranges for predicted rates of ET reactions between the hemes were estimated under the assumption that both ΔG^0_{DA} and ΔG^0_{DH} are in the range of −0.15 to 0.15 eV.

*$k_{hopping} = 1/\tau_{hopping}$; $k_{tunneling} = 1/\tau_{tunneling}$. The range for $\tau_{hopping}$ is determined from the triangular region outlined by the dotted lines on each hopping map. The range for $\tau_{tunneling}$ is determined based on the corresponding $\tau_{hopping}$ values on the upper right borderline, where $\tau_{hopping}$ is equal to $\tau_{tunneling}$.

†Ranges for $k_{tunneling}$ with $Heme_{6C}$ or $Heme_{5C}$ as the electron donor are identical.

ET reactions between the two hemes with Trp93 as the hopping site to examine the effects of these parameters as well as H_{AB}. The hopping map is a contour plot of $-\log_{10}(\tau_{hopping})$ against ΔG^0_{DA} and ΔG^0_{DH}, where τ is the average ET time, ΔG^0_{DA} is the driving force for the overall ET process from the donor to the acceptor, and ΔG^0_{DH} is the driving force for the first hopping step from the donor (i.e., one of the hemes) to the hopping site (i.e., Trp93). There are two blank regions on the map representing scenarios in which hopping cannot occur. The upper right corner is the region in which single-step tunneling is calculated to be faster than hopping ($\tau_{hopping} > \tau_{tunneling}$), and the bottom left corner is the region in which ΔG^0_{DA} is larger than ΔG^0_{DH} (the hopping site is an electron/hole sink).

In *bis*-Fe(IV) MauG, the precise $\Delta G°$ value of the ET reactions between the hemes are unknown as the two consecutive E_m values for the *bis*-Fe(IV)/diferric MauG redox couple are not known. However, the E_m values for Fe(IV)/Fe(III) redox couples in many heme-dependent peroxidases have been determined to be in the range of 724–1,040 mV (36) and are similar to the values for compound I/II redox couples (802–1156 mV) (36) as well as the values for $Trp^{+\bullet}$/Trp redox couples (890–1,080 mV) (41). These values suggest that $\Delta G°$ of ET reactions between the hemes in *bis*-Fe(IV) MauG is near zero. If hopping via Trp93 is involved, $\Delta G°$ of each hopping segment is also near zero. This is consistent with the observation that both Fe(IV) hemes and the Trp93 radical are in redox equilibrium. Thus, in interpreting these hopping maps it was assumed that both ΔG^0_{DA} and ΔG^0_{DH} are in the range of −0.15 to 0.15 eV (see the triangular region outlined by the dashed lines on each map). The λ value used to construct the hopping maps also is unknown in the ET system of *bis*-Fe(IV) MauG. Instead of a specific value [0.7 or 0.8 eV as conventionally used in intraprotein ET predictions (40, 42)], a range of values from 0.6 to 1.0 eV was tested. During the interconversion between the resonance structures of Cpd I and Cpd I′ shown in Fig. 4*C*, there are two consecutive one-electron ET reactions between the hemes: from Cpd I (Cpd I′) to *bis*-Fe(IV) and from *bis*-Fe(IV) to Cpd I′(Cpd I). The hopping map study cannot distinguish these two ET reactions because they share the same ET path and the same redox centers, including the electron donor, the electron acceptor, and the hopping site. Although the electron donor and acceptor are at different redox states in these two cases, the hopping map study is unbiased because the ΔE_m values of ET reactions, rather than the absolute E_m values of each individual redox center, are what determine the results.

Fig. 5*A* shows a hopping map constructed with $Heme_{6C}$ as the electron donor and $Heme_{5C}$ as the electron acceptor at λ = 0.8 eV. This map may be used to examine both the ET reaction converting Cpd I to *bis*-Fe(IV) and the ET reaction converting *bis*-Fe(IV) to Cpd I′. The ET rate between the hemes is estimated to be $7.2 \times 10^6 - 5.0 \times 10^8$ s^{-1} when Trp93-mediated hopping is involved in the ET reactions (Table 2). In contrast, single-step tunneling with ΔG^0_{DA} in the same range is much slower, with the rate constant estimated to be $8.5 \times 10^2 - 6.5 \times 10^3$ s^{-1}. With λ varying from 0.6 to 1.0 eV, the ET rate for both the Trp93-mediated hopping pathway and the single-step tunneling pathway increases as λ decreases, and decreases as λ increases (Fig. 5 and Table 2). In each case, the hopping mechanism leads to an increase of four to five orders of magnitude in the ET rate vs. direct tunneling (Table 2). This is in reasonable agreement with the HARLEM analysis, which predicted a difference of approximately six orders of magnitude in the ET rate. The same conclusions were obtained from the hopping maps constructed with $Heme_{5C}$ as the electron donor and $Heme_{6C}$ as the electron acceptor. Despite no advantage in the driving force, hopping via Trp93 may enhance the ET rate considerably by substantially decreasing the effective ET distance and increasing the effective electronic coupling element compared with single-step direct tunneling. A point of critical significance is that the hopping maps predict ET rates greater than 10^7 s^{-1} for the hopping mechanism. As stated earlier, model studies suggest that rate constants in the range of 10^7–10^{11} s^{-1} are essential for delocalization of the spin and charge within CR complexes (3–5). Thus, a hole-hopping mechanism for ET between the hemes mediated by Trp93 can explain the observed CR-transition phenomenon in *bis*-Fe(IV) MauG in the absence of direct contact between the hemes. It is interesting to note that ET via hole hopping also is suggested to occur between *bis*-Fe(IV) MauG and the tryptophan residues being oxidized in preMADH via a tryptophan residue located at the interface of the MauG–preMADH complex (25, 40).

Conclusions

This work describes a CR-transition phenomenon involving two hemes in an enzyme-based high-valence catalytic Fe intermediate. CR-transition phenomena reported in model systems usually require irradiation or electrochemical oxidation to produce the CR complexes and low temperatures for stabilization (1, 2, 5, 6, 29, 30),

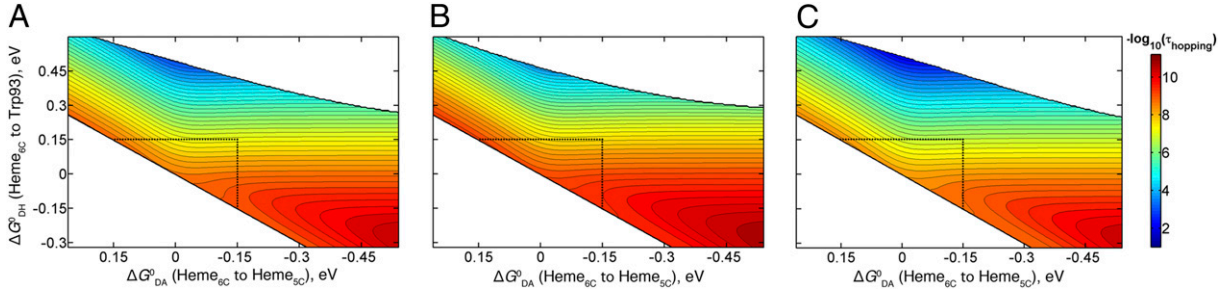

Fig. 5. Hopping maps for the ET reactions between the hemes. These hopping maps were constructed with Trp93 as the hopping site, $Heme_{6C}$ as the electron donor, and $Heme_{5C}$ as the electron acceptor at 298 K with (*A*) λ = 0.8 eV, (*B*) λ = 0.6 eV, and (*C*) λ = 1.0 eV. The ET parameters used to construct the hopping maps, i.e., the distance (*r*) and the decay constant (β), were adopted from the results of the HARLEM calculation in Table 1. The dashed lines indicate ΔG^0 at ±0.15 eV.

whereas the CR complex of MauG is relatively stable under physiologically relevant conditions. The CR complex of MauG is a ternary system composed of two physically separated hemes and a tryptophan residue, unlike those in model systems. A hopping-mediated CR model is proposed in which very rapid and reversible ET between the hemes, with an intervening tryptophan as the hopping site, mimics the distribution of the spins and charges that one would observe in an extended conjugated system. The identification of the spectroscopic signature of this CR phenomenon will be useful in identifying similar CR interactions in other biological systems.

Methods

Protein Expression and Purification. Wild-type, W199F, P107V, and Y294H MauG was expressed in *Paracoccus denitrificans*. PreMADH was expressed in *Rhodobacter sphaeroides*. These proteins were purified as described previously (9, 13, 16, 25, 26).

Vis-NIR Absorption Spectroscopy. The optical spectra of MauG were recorded aerobically on a Cary 5000 UV-Vis-NIR spectrophotometer at room temperature in 50 mM potassium phosphate buffer, pH 7.5. The concentration of H_2O_2 was determined based on the molar absorptivity of 43.6 $M^{-1}{\cdot}cm^{-1}$ at 240 nm.

ET Pathway Prediction. The HARLEM program, developed by Kurnikov (http://harlem.chem.cmu.edu/index.php), was used to analyze the ET pathway between the two hemes of MauG based on the crystal structure (10). The ET parameters, including the decay constants (β) and the relative values of electronic coupling element (H_{AB}), for the single-step tunneling mechanism and the two-step Trp93-mediated hopping mechanism were calculated using the direct distance approach of Dutton and coworkers (42). When defining redox centers, the iron–porphyrin complexes without the propionate groups of the hemes, and the indole moiety without the amino acid backbone of Trp93, were selected.

Hopping Map Construction. The MATLAB program for hopping map construction was obtained from the Beckman Institute Laser Resource Center (www.bilrc.caltech.edu) (40). The parameters used to construct the hopping maps consist of the temperature (T), the reorganization energy (λ), the distances (r), and the decay constants (β) for the single-step tunneling pathway as well as each hopping segment. The temperature was set at 298 K; λ was varied from 0.6 to 1.0 eV to examine its effect on the ET process. The values of r and β were adopted from the results of the HARLEM calculation in Table 1.

ACKNOWLEDGMENTS. We thank Drs. Laren M. Tolbert and Kyril Solntsev (Georgia Institute of Technology) for providing access to the UV-Vis-NIR spectrophotometer. This work was supported by National Science Foundation Grant MCB0843537 (to A.L.), National Institutes of Health Grant GM041574 (to V.L.D.), and the Georgia Research Alliance–Georgia Cancer Coalition Distinguished Scholar program (A.L.). J.G. acknowledges fellowship support from the Molecular Basis of Disease program of Georgia State University. K.D. acknowledges fellowship support from the Southern Regional Education Board.

1. Badger B, Brocklehurst B (1968) Formation of dimer cations of aromatic hydrocarbons. *Nature* 219(5151):263–265.
2. Magueres PL, Lindeman SV, Kochi JK (2000) Novel (Heteromolecular) π-complexes of aromatic cation radicals. Isolation and structural characterization. *Org Lett* 2(23):3567–3570.
3. Lindeman SV, Rosokha SV, Sun DL, Kochi JK (2002) X-ray structure analysis and the intervalent electron transfer in organic mixed-valence crystals with bridged aromatic cation radicals. *J Am Chem Soc* 124(5):843–855.
4. Rosokha SV, Sun DL, Kochi JK (2002) Conformation, distance, and connectivity effects on intramolecular electron transfer between phenylene-bridged aromatic redox centers. *J Phys Chem A* 106(10):2283–2292.
5. Sun DL, Rosokha SV, Lindeman SV, Kochi JK (2003) Intervalence (charge-resonance) transitions in organic mixed-valence systems. Through-space versus through-bond electron transfer between bridged aromatic (redox) centers. *J Am Chem Soc* 125(51):15950–15963.
6. Błoch-Mechkour A, Bally T, Marcinek A (2011) Dimer radical cations of indole and indole-3-carbinol: Localized and delocalized radical cations of diindolylmethane. *J Phys Chem A* 115(26):7700–7708.
7. Breton J, Nabedryk E, Parson WW (1992) A new infrared electronic transition of the oxidized primary electron donor in bacterial reaction centers: A way to assess resonance interactions between the bacteriochlorophylls. *Biochemistry* 31(33):7503–7510.
8. Kanchanawong P, et al. (2006) Charge delocalization in the special-pair radical cation of mutant reaction centers of *Rhodobacter sphaeroides* from Stark spectra and nonadiabatic spectral simulations. *J Phys Chem B* 110(37):18688–18702.
9. Wang YT, et al. (2003) MauG, a novel diheme protein required for tryptophan tryptophylquinone biogenesis. *Biochemistry* 42(24):7318–7325.
10. Jensen LMR, Sanishvili R, Davidson VL, Wilmot CM (2010) In crystallo posttranslational modification within a MauG/pre-methylamine dehydrogenase complex. *Science* 327(5971):1392–1394.
11. Fu R, Liu F, Davidson VL, Liu A (2009) Heme iron nitrosyl complex of MauG reveals an efficient redox equilibrium between hemes with only one heme exclusively binding exogenous ligands. *Biochemistry* 48(49):11603–11605.
12. Yukl ET, et al. (2013) Diradical intermediate within the context of tryptophan tryptophylquinone biosynthesis. *Proc Natl Acad Sci USA* 110(12):4569–4573.
13. Li X, et al. (2008) A catalytic di-heme *bis*-Fe(IV) intermediate, alternative to an Fe(IV)=O porphyrin radical. *Proc Natl Acad Sci USA* 105(25):8597–8600.
14. Li XH, Feng ML, Wang YT, Tachikawa H, Davidson VL (2006) Evidence for redox cooperativity between *c*-type hemes of MauG which is likely coupled to oxygen activation during tryptophan tryptophylquinone biosynthesis. *Biochemistry* 45(3):821–828.
15. Lee S, Shin S, Li X, Davidson VL (2009) Kinetic mechanism for the initial steps in MauG-dependent tryptophan tryptophylquinone biosynthesis. *Biochemistry* 48(11):2442–2447.
16. Tarboush NA, et al. (2010) Functional importance of tyrosine 294 and the catalytic selectivity for the *bis*-Fe(IV) state of MauG revealed by replacement of this axial heme ligand with histidine. *Biochemistry* 49(45):9783–9791.
17. Jensen LMR, et al. (2012) Geometric and electronic structures of the His-Fe(IV)=O and His-Fe(IV)-Tyr hemes of MauG. *J Biol Inorg Chem* 17(8):1241–1255.
18. Que L, Jr. (2007) The road to non-heme oxoferryls and beyond. *Acc Chem Res* 40(7):493–500.
19. Decker A, Rohde JU, Que L, Jr., Solomon EI (2004) Spectroscopic and quantum chemical characterization of the electronic structure and bonding in a non-heme Fe^{IV} = O complex. *J Am Chem Soc* 126(17):5378–5379.
20. Orgel LE (1966) *An Introduction to Transition-Metal Chemistry: Ligand-Field Theory* (Methuen, London), 2nd Ed.
21. Wittenberg BA, Kampa L, Wittenberg JB, Blumberg WE, Peisach J (1968) The electronic structure of protoheme proteins. II. An electron paramagnetic resonance and optical study of cytochrome *c* peroxidase and its derivatives. *J Biol Chem* 243(8):1863–1870.
22. Hewson WD, Hager LP (1979) Oxidation of horseradish peroxidase compound II to compound I. *J Biol Chem* 254(9):3182–3186.
23. Lardinois OM, Ortiz de Montellano PR (2004) Autoreduction of ferryl myoglobin: Discrimination among the three tyrosine and two tryptophan residues as electron donors. *Biochemistry* 43(15):4601–4610.
24. Makris TM, von Koenig K, Schlichting I, Sligar SG (2006) The status of high-valent metal oxo complexes in the P450 cytochromes. *J Inorg Biochem* 100(4):507–518.
25. Tarboush NA, et al. (2011) Mutagenesis of tryptophan199 suggests that hopping is required for MauG-dependent tryptophan tryptophylquinone biosynthesis. *Proc Natl Acad Sci USA* 108(41):16956–16961.
26. Feng M, et al. (2012) Proline 107 is a major determinant in maintaining the structure of the distal pocket and reactivity of the high-spin heme of MauG. *Biochemistry* 51(8):1598–1606.
27. Heckmann A, Lambert C (2012) Organic mixed-valence compounds: A playground for electrons and holes. *Angew Chem Int Ed* 51(2):326–392.
28. Hausser KH, Murrell JN (1957) Pi complexes between organic free radicals. *J Chem Phys* 27(2):500–504.
29. Fajer J, Borg DC, Forman A, Dolphin D, Felton RH (1970) π-Cation radicals and dications of metalloporphyrins. *J Am Chem Soc* 92(11):3451–3459.
30. Fuhrhop JH, Wasser P, Riesner D, Mauzerall D (1972) Dimerization and bonding of a zinc porphyrin cation radical. Thermodynamics and fast reaction kinetics. *J Am Chem Soc* 94(23):7996–8001.
31. Brancato-Buentello KE, Kang SJ, Scheidt WR (1997) Metalloporphyrin mixed-valence π cation radicals: Solution stability and properties. *J Am Chem Soc* 119(12):2839–2846.
32. Lü JM, Rosokha SV, Kochi JK (2003) Stable (long-bonded) dimers via the quantitative self-association of different cationic, anionic, and uncharged π-radicals: Structures, energetics, and optical transitions. *J Am Chem Soc* 125(40):12161–12171.
33. Takai A, Gros CP, Barbe JM, Guilard R, Fukuzumi S (2009) Enhanced electron-transfer properties of cofacial porphyrin dimers through π-π interactions. *Chem Eur J* 15(13):3110–3122.
34. Bockman TM, Kochi JK (1990) Isolation and oxidation-reduction of methylviologen cation radicals. Novel disproportionation in charge-transfer salts by X-ray crystallography. *J Org Chem* 55(13):4127–4135.
35. Song H, Orosz RD, Reed CA, Scheidt WR (1990) Dimerization of metalloporphyrin π cation radicals. Characterization of two novel dimers: $[Zn(OEP^{\bullet})(OH_2)]_2(ClO_4)_2$ and $[Ni(OEP)]_2(ClO_4)_2$. *Inorg Chem* 29:4274–4282.
36. Battistuzzi G, Bellei M, Bortolotti CA, Sola M (2010) Redox properties of heme peroxidases. *Arch Biochem Biophys* 500(1):21–36.
37. Baldwin J, et al. (2000) Mechanism of rapid electron transfer during oxygen activation in the R2 subunit of *Escherichia coli* ribonucleotide reductase. 1. Evidence for a transient tryptophan radical. *J Am Chem Soc* 122(49):12195–12206.
38. Byrdin M, Villette S, Eker AP, Brettel K (2007) Observation of an intermediate tryptophanyl radical in W306F mutant DNA photolyase from *Escherichia coli* supports electron hopping along the triple tryptophan chain. *Biochemistry* 46(35):10072–10077.
39. Marcus RA, Sutin N (1985) Electron transfers in chemistry and biology. *Biochim Biophys Acta* 811(3):265–322.
40. Warren JJ, Ener ME, Vlček A, Jr., Winkler JR, Gray HB (2012) Electron hopping through proteins. *Coord Chem Rev* 256(21-22):2478–2487.
41. DeFelippis MR, Murthy CP, Faraggi M, Klapper MH (1989) Pulse radiolytic measurement of redox potentials: The tyrosine and tryptophan radicals. *Biochemistry* 28(11):4847–4853.
42. Page CC, Moser CC, Chen X, Dutton PL (1999) Natural engineering principles of electron tunnelling in biological oxidation-reduction. *Nature* 402(6757):47–52.